Water Science & Technology

Water Science & Technology Vol 93 No 4, 469 doi: 10.2166/wst.2026.218

Inlet modifications for increased box culvert capacity: a numerical modelling approach

Thea Maria Dorothea Giliomee *, Ione Loots and Marco van Dijk

Department of Civil Engineering, University of Pretoria, Lynnwood Road, Hatfield, Pretoria, South Africa
*Corresponding author. E-mail: u20424028@tuks.co.za

TMDG, 0009-0004-1582-6865; IL, 0000-0003-0715-6852; MvD, 0000-0002-3830-526X

ABSTRACT

Inlet modifications applied to culverts can increase the culvert discharge capacity, which will help stormwater drainage systems adapt to larger flood events. Wingwalls and headwalls are already widely used as retaining structures. It is therefore feasible to optimise these inlet structures to increase culvert capacity. Building upon previous physical modelling research, this study evaluated a wider range of headwall and wingwall angle combinations to refine the findings. Headwalls and wingwalls were compared with rounded-edge box culvert inlets with the aim of improving capacity under inlet control. Numerical modelling was used to optimise wingwalls and headwalls and rounded-edge inlets, quantify their improvement, and verify the alignment of results with established references and guidelines. A 15° headwall with a 15° wingwall added to a box culvert improved the flow by up to 34% at a headwater depth of twice the culvert height (2*D*), or up to 26% at 1.2*D*. This solution provides the best balance between hydraulic performance and practical implementation. The largest improvement obtained by rounding the edges of a square box culvert is 30% at 2*D*. Inlet modifications provide a sustainable solution to increase culvert drainage capacity, which can mitigate flood risks.

Key words: CFD, computational fluid dynamics, flood control, hydraulic capacity, hydraulic structures, stormwater drainage

HIGHLIGHTS

- Modified inlets can be used to adapt culverts to increased peak floods.
- Numerical modelling presents an opportunity to test multiple combinations.
- The smallest wingwall and headwall angles provide the greatest flow improvement.
- Wingwalls and headwalls are more effective than rounded-edge inlets for box culverts.
- Discharge capacity improvements were quantified for each inlet configuration.

INTRODUCTION

Culverts are used as an integral component of stormwater management systems to convey specific design flows. However, they often discharge a smaller capacity than expected (Straub *et al.* 1953). This is attributed to flow contraction just after the culvert inlet (Schall *et al.* 2012). Culverts can also become insufficient over time due to increasing flood peaks (Cullis *et al.* 2015), due to climate change (van der Werf *et al.* 2025) and urban development (Amback *et al.* 2025). Other factors, such as sediment accumulation, can significantly reduce culvert flow capacity by narrowing the cross-sectional area and increasing hydraulic resistance (Quang *et al.* 2022). High flows can also transport debris that accumulates at culvert inlets, causing reduced hydraulic performance (Bradley *et al.* 2005). Inadequate culvert drainage can lead to infrastructure damage and unsafe conditions for road users, both during and after flood events.

Rather than adding barrels to an inadequate culvert, discharge capacity can be improved by minimising flow contraction at the inlet through a more gradual transition (Yarnell *et al.* 1926; Schall *et al.* 2012; Jaeger 2019; Giliomee *et al.* 2025). Inlet modifications would either increase the culvert capacity for a specific headwater depth or pass the design discharge at a lower headwater depth (Harrison *et al.* 1972). Increased flushing discharge has been shown to improve sediment removal efficiency in drainage systems (Feng *et al.* 2023). Similarly, culvert inlet modifications might help limit sediment accumulation by improving the culvert's discharge capacity and reducing low-velocity zones at the inlet.

Headwalls and wingwalls are already widely used as retaining structures for unstable embankments (Morrow 2020). They provide structural support, protecting the culvert from erosion and piping (Schall *et al.* 2012; Jaeger 2019). Therefore, it is feasible to optimise wingwalls and headwalls to improve discharge capacity, while protecting the culvert. Previous research showed that:

- A 15° headwall provided the greatest discharge improvement under all conditions: for box culverts, the increases were 16% under free-outlet flow and 11% under submerged-outlet flow, while for circular culverts the improvements were 7 and 9%, respectively (Ashour *et al.* 2016). The hydraulic efficiency of a circular culvert was also shown to increase by up to 20.1% at $H_1/D = 2.25$ (Aly 2017).
- Wingwall angles between 19 and 75° have been used on box culverts (Buck & Allitt 2019), with 30 and 45° being the most commonly used angles in practice (West 1956). In corrugated-metal pipes, 45° wingwalls increased discharge by about 1–10% (Yarnell *et al.* 1926).

Most studies have examined wingwall and headwall angles individually or at the same angles when combined, as seen in the work of de Jager & van Dijk (2024). However, only limited investigation has been conducted on the use of different angles in combinations of wingwalls and headwalls, using physical modelling (Giliomee *et al.* 2025). In addition, limited previous research has shown that culvert inlets rounded to at least 0.15B (culvert width) (Jaeger 2019) or to 0.15D (culvert height) (Straub *et al.* 1953) increase culvert performance. The dimensions B and D are illustrated in Figure 1(a), and the rounding radius R is shown in Figure 1(b) for clarity. However, no previous data is available on the optimal rounding radius for box culverts.

Considering the expected construction difficulties associated with rounded inlets for box culverts, it is useful to also compare the improvement potential of rounded inlets with improvement gained with angled wingwalls and headwalls. The practicality of installing improved inlets relative to their flow improvement has also not yet been considered, which is important when upgrading the culvert as a whole and accounting for different factors.

This study aimed to address these research gaps by refining the inlet modifications for box culverts under inlet control. The first objective was to ensure the numerical modelling results are calibrated with physical modelling results, building upon a previous study. The second objective was to verify that the numerical modelling results align with previous research data for the standard square-edge inlets. The third objective was to optimise wingwall and headwall configurations as well as rounded-edge inlets for square box culverts, considering both hydraulic and practical aspects. The fourth objective was to quantify the discharge capacity improvements for each inlet type.

METHODS

Numerical replication of the physical modelling

ScFLOW, a Computational Fluid Dynamics (CFD) software developed by Hexagon under its Cradle CFD suite, was used to evaluate different inlet configurations for square box culverts. The CFD model setup replicates the culvert in the hydraulic flume, as shown in Figure 2(a), where physical studies on inlet modifications were previously performed (Giliomee *et al.*

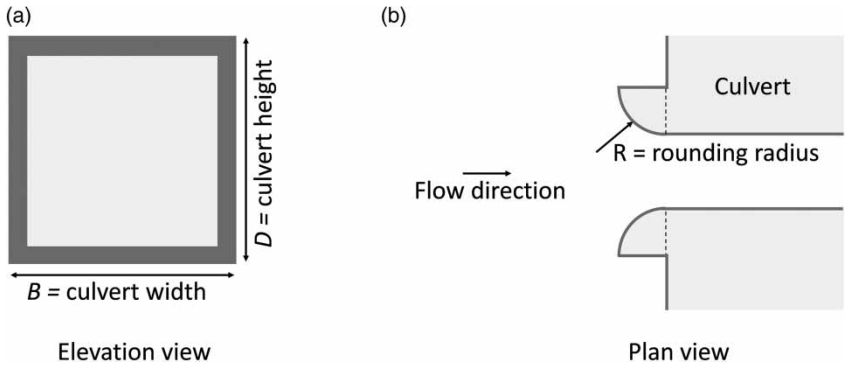

Figure 1 | (a) Elevation view of the box culvert showing the width (B) and height (D) of a culvert, (b) plan view showing the rounding radius (R) for the rounded-edge inlet.

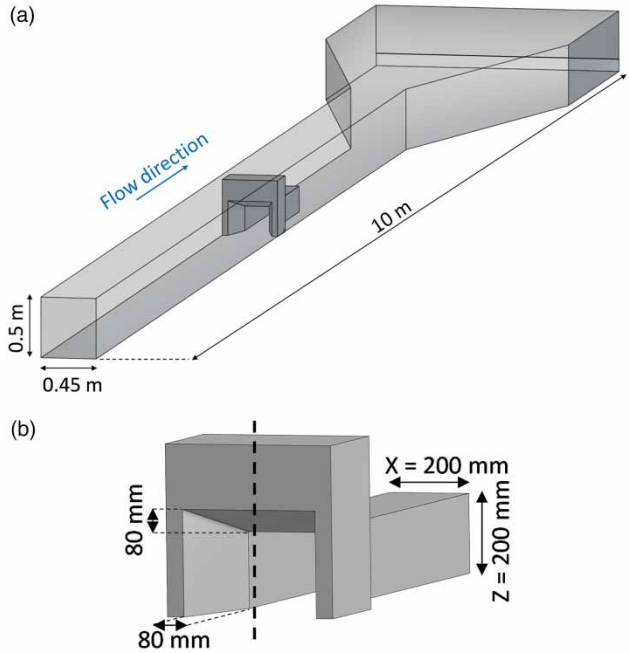

Figure 2 | (a) Physical modelling flume and culvert setup, and (b) 15° wingwall and 15° headwall box culvert model.

2025). The physical modelling flume had glass sidewalls and a metal floor. The flume slope was set to 1%, which is the minimum proposed slope to prevent silt deposition at culverts (SANRAL 2013) and to ensure inlet control conditions, since the inlet geometry has a greater influence on the flow through the barrel than under outlet control (West 1956; Jones *et al.* 2006).

Figure 2(b) shows the 3D CAD model of the 200 × 200 mm box culvert with a 15° wingwall and 15° headwall, provided as an example to illustrate the geometry and dimensions of the physical model culverts that were replicated. The culvert models were made as large as possible within the flume limits to minimise surface tension effects. For all the models, the wingwalls extended 0.4*D* (80 mm) to the sides of the barrel, and the headwall extended 0.4*D* (80 mm) upward. This ensured that the enlarged inlet cross-sectional area remained constant.

During the physical modelling experiments conducted by Giliomee *et al.* (2025), each culvert inlet configuration was placed in the hydraulic flume, and the headwater depth was measured for 20 flow rates ranging from 5 to 83 L/s.

A 1:3 geometric scale was used in Giliomee *et al.* (2025), where the 200 × 200 mm model represents a commonly used 600 × 600 mm prototype precast concrete box culvert (Rocla 2017). In the physical study, Froude similarity was applied, and Reynolds numbers exceeded 86,000, ensuring fully turbulent flow where flow resistance remains nearly constant despite further increases in Reynolds number. The CFD simulations therefore used the same model-scale geometry and discharge range to enable direct comparison with measured headwater depths while remaining representative of the prototype culvert. For the numerical model, flow rates between 3 and 78 l/s were tested, corresponding to approximately 47–1,215 l/s for a 600 × 600 mm prototype box culvert.

The physical modelling study tested five inlet configurations: 90° wingwall with 90° headwall, 30° wingwall with 15° headwall, 30° wingwall with 30° headwall, 45° wingwall with 45° headwall, and 45° wingwall with 15° headwall. These five configurations were then replicated in the numerical modelling to calibrate the CFD models. After calibration, additional numerical models were developed to investigate a wider range of wingwall and headwall angles, as well as rounded-edge inlets, allowing a wider range of inlet designs to be assessed than would be feasible in physical testing.

Numerical modelling of additional inlet configurations

The different wingwall and headwall configurations tested with numerical modelling are presented in Table 1. A 90° wingwall and 90° headwall configuration represents the standard square-edge inlet.

Wingwalls can be used to increase hydraulic efficiency if designed as a side-tapered inlet (Morrow 2020). Therefore, the wingwalls and headwalls were modelled as tapered inlets, by extending them until they intersected. The different rounded-edge inlet configurations tested were:

Table 1 | Different wingwall and headwall angles tested with CFD analysis

		Headwall angle						
		0°	5°	15°	30°	45°	60°	90°
Wingwall angle	0°	X						
	5°		X					
	15°		X	X				
	30°		X	X	X			
	45°		X	X		X		
	60°		X		X		X	
	90°							X

- 0.05D rounded-edge
- 0.15D rounded-edge
- 0.25D rounded-edge
- 0.35D rounded-edge
- 0.45D rounded-edge

For numerical modelling, each 3D CAD model consisting of the culvert with an inlet modification inside the modelled hydraulic flume was imported into the scFLOW Pre-Processor, where the simulation model was built. Since the experiment was symmetrical about the *zy*-plane, the entire simulation model was split in half, as shown in Figure 3, and a free-slip boundary condition was applied along the symmetry plane. The fluid region was defined to envelop the entire culvert.

The different boundary conditions are provided in Table 2. Air was used as the initial fluid in the domain, and water entered through the flume inlet at a specified constant mass flow rate. Different flow rates were tested for each inlet configuration. The

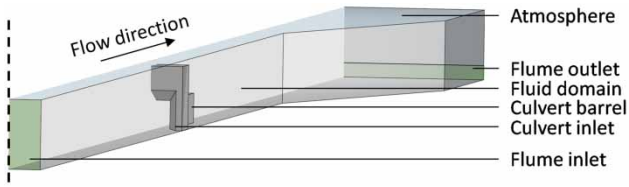

Figure 3 | Half-flume and culvert simulation setup.

Table 2 | Boundary conditions used in the CFD simulations

Boundary/region	Type of boundary condition	Details
Symmetry plane (zy-plane)	Free-slip boundary	Used because the experiment is symmetric; half-model used
Inlet (flume inlet)	Mass flow inlet	Water enters at constant mass flow rate At least nine flow rates tested: 3–83 l/s (full flume), 1.5–41.5 l/s (half-flume)
Outlet	Outflow/static pressure	Static pressure of 0 Pa at outlet allowing both air and water to exit the domain naturally
Atmospheric interface/free surface	Pressure boundary	Gas region with 0 Pa gauge pressure (atmospheric)
Culvert walls	Wall boundary (rigid)	Initially roughness = 0.002 m Adjusted during calibration, final roughness = 0.003 m
Glass sidewalls	Wall boundary (rigid)	Initially roughness = 0.0000015 m Adjusted during calibration, final roughness = 0.003 m
Painted metal floor and walls	Wall boundary (rigid)	Initially roughness = 0.0002 m Final: no-slip boundary with zero roughness

equivalent sand-grain roughness heights (k_s) for the culvert, glass sidewalls, and metal floor were calibrated to align with the results from the five configurations tested in the physical modelling study (90° wingwall and 90° headwall, 30° wingwall and 15° headwall, 30° wingwall and 30° headwall, 45° wingwall and 45° headwall, and 45° wingwall and 15° headwall). Initial roughness values were chosen; however, the simulated headwater level for the standard square-edge inlet (90° wingwall and 90° headwall) was higher than observed in the physical modelling study, while the simulated headwater level for the best-performing configuration in the physical modelling study (30° wingwall and 15° headwall) was much lower than expected. Therefore, the roughness of the culvert was systematically increased with each iteration, while the roughness of the glass and metal surfaces was decreased, until the headwater levels for six different flow rates fell within a statistically acceptable range across all five calibration cases. The initial and final roughness values are given in Table 2.

The fundamental flow physics were solved using the incompressible continuity equation (Equation (1)) and the Navier-Stokes momentum equation (Equation (2)) (Versteeg & Malalasekera 2007):

$$\nabla \cdot \mathbf{u} = 0 \tag{1}$$

where:

$\mathbf{u}$ = velocity vector (m/s)

$$\rho\left(\frac{\partial \mathbf{u}}{\partial t} + \mathbf{u} \cdot \nabla \mathbf{u}\right) = -\nabla p + \nabla \cdot [\mu(\nabla \mathbf{u} + (\nabla \mathbf{u})^T)] + \rho \mathbf{g} \tag{2}$$

where ρ = fluid density (kg/m^3); $\mathbf{u}$ = velocity vector (m/s); p = pressure (Pa); μ = molecular viscosity (Pa·s); $\mathbf{g}$ = gravitational acceleration vector (m/s^2).

Reynolds-Averaged Navier-Stokes (RANS) can be applied to complex industrial problems (Simscale 2025), as done in Dutta *et al.* (2021) and Martin *et al.* (2023). Therefore, turbulent flow was modelled using the RANS equations together with the Shear Stress Transport (SST) $k-\omega$ turbulence model. The SST $k-\omega$ model solves transport equations for the turbulent kinetic energy, k, and the specific dissipation rate, ω (Menter 1994). The turbulent viscosity is computed using the standard $k-\omega$ relation (Equation (3)) (Menter 1994), with the SST blending and limiter terms applied automatically within the solver to contribute to the effective viscosity used in the momentum equation:

$$\mu_t = \frac{\rho k}{\omega} \tag{3}$$

where μ_t = turbulent (eddy) viscosity (Pa·s); k = turbulent kinetic energy (m^2/s^2); ω = specific dissipation rate (1/s).

The $k-\omega$ SST model is widely recognised as an industry-standard turbulence model (Marum *et al.* 2021; Iwamoto *et al.* 2023), since it provides better prediction of flow separation (Simscale 2025). The free-surface behaviour of the air-water flow was captured using the Volume of Fluid (VOF) method with interface reconstruction performed using the Fine Interface Reconstruction Method (FIRM) implemented in scFLOW. The interface was tracked using the VOF transport equation (Hirt & Nichols 1981), (Equation (4)):

$$\frac{\partial \alpha}{\partial t} + \mathbf{u} \cdot \nabla \alpha = 0 \tag{4}$$

where α = water volume fraction (–); $\mathbf{u}$ = velocity vector (m/s).

In the VOF model, mixture viscosity is obtained using arithmetic averaging, and the mixture density is computed from the water volume fraction using the mixture-property relation (Hexagon 2024) (Equation (5)):

$$\rho = \alpha \rho_w + (1-\alpha)\rho_a \tag{5}$$

where ρ_w = density of water (kg/m^3); ρ_a = density of air (kg/m^3); α = water volume fraction (–).

A transient CFD simulation was used because the headwater depth fluctuated during the solution process and needed to be compared with the ± 10 mm fluctuations observed in the physical model, capturing the time-dependent behaviour of the flow

(Ueyama 2019). Furthermore, flow separation and vortex formation at the culvert inlet are inherently unsteady and therefore require unsteady RANS modelling for realistic prediction (Iaccarino *et al.* 2003).

A three-level grid convergence analysis was carried out for a representative culvert inlet configuration (30° wingwall and 15° headwall) at three discharges (25.2, 51.0 and 80.8 l/s) to assess mesh independence, following the procedure of Celik *et al.* (2008). The coarse, medium and fine meshes contained 16,513, 35,053 and 89,659 cells (N), respectively. For each discharge, the headwater depth values (Φ) computed on the coarse, medium and fine grids were used to evaluate the apparent order of accuracy (p) and the Grid Convergence Index (GCI). The apparent order, p, was obtained iteratively from the three-grid relations in Celik *et al.* (2008). The fine-grid GCI was then calculated using Equation (6), based on the grid refinement ratio, r, defined in Equation (7), as described in Celik *et al.* (2008):

$$\mathrm{GCI}_{\mathrm{fine}}^{21} = \frac{1.25|\Phi_{\mathrm{fine}} - \Phi_{\mathrm{medium}}|}{|\Phi_{\mathrm{fine}}|(r_{21}^{p} - 1)} \tag{6}$$

$$r_{21} = \left(\frac{N_{\mathrm{fine}}}{N_{\mathrm{medium}}}\right)^{1/3}, \quad r_{32} = \left(\frac{N_{\mathrm{medium}}}{N_{\mathrm{coarse}}}\right)^{1/3} \tag{7}$$

A summary of the results is provided in Table 3.

For the lowest discharge (25.2 l/s), Table 3 shows a fine-grid GCI of 6.6% and a medium-grid GCI of 8.36%, indicating that this case is not fully in the asymptotic range of convergence and carries higher numerical uncertainty. However, the headwater differences between meshes are small (<4.5 mm or ~1%), and with the inlet unsubmerged in this flow condition, the headwater is only mildly sensitive to mesh refinement. At 51.0 and 80.8 l/s, the fine-grid GCI values are <1%, as shown in Table 3, demonstrating excellent or acceptable mesh independence in the main operating range. The 51.0 l/s case shows clear asymptotic convergence with negligible discretisation error, while the slight oscillatory behaviour at 80.8 l/s still results in a fine-grid GCI <0.5% and therefore acceptably small numerical uncertainty. These results indicate that the fine mesh provides sufficiently converged solutions for the inlet models considered, and it was therefore used for all further simulations.

A final mesh base size of 50 mm was used, with local refinement to 25 mm near the inlet, outlet, and around the culvert. The same cell sizes were applied to all culvert inlet models, resulting in a total mesh size of 84,000–90,000 cells. For the rounded-edge inlets, small faceting adjustments were made to maintain smooth curvature without changing the mesh density, ensuring that performance differences were due to geometry rather than meshing. This allowed direct comparison between the models. Figure 4 shows the final polyhedral volume mesh used for all simulations, as polyhedral elements provide improved numerical accuracy and stability with fewer cells than tetrahedral meshes.

The simulation was run with a time step of 0.01 s for a total of 15,000 time steps. Each steady-state simulation (one culvert inlet and one flow rate) required approximately 8–10 h on a desktop computer with an 8-core CPU (Intel Core i7-9700K@ 3.6 GHz) and 32 GB RAM. On a laptop system with a 4-core CPU (Intel Core i5-12540H) and 16 GB RAM, the same simulations required 13–15 h. All simulations were executed using parallel computation utilising all available CPU cores. Each model analysis began with a low flow rate, and the corresponding water depth was measured just upstream of the culvert inlet, measuring headwater, H_1. The final H_1 value used for calculations was the average headwater level over the last 1,000 time steps after the water level stabilised. The flow was incrementally increased, re-analysed and the same measurement procedure followed until the headwater depth reached a maximum of 2D. This process was repeated for each culvert inlet model, with the average Courant number remaining close to one across all simulations. A third-degree polynomial trendline

Table 3 | Grid convergence results for headwater depth

Q, Flow (l/s)	Headwater depth, Φ_1, fine (mm)	Headwater depth, Φ_2, medium (mm)	Headwater depth, Φ_3, coarse (mm)	Order of accuracy, p	$\mathrm{GCI}_{\mathrm{fine}\ (21)}$ (%)	$\mathrm{GCI}_{\mathrm{medium}(32)}$ (%)
25.19	170.93	168.68	166.49	0.71	6.61	8.36
51.03	272.69	271.43	263.41	7.64	0.06	0.64
80.81	435.55	434.74	435.19	1.65	0.35	0.26

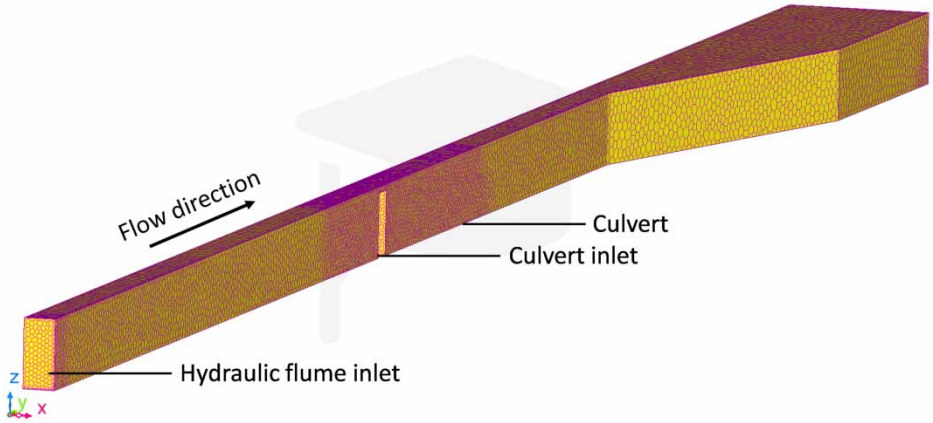

Figure 4 | Polyhedral mesh with local refinement at the culvert, inlet and outlet.

fitted to the flow versus headwater depth values obtained made it possible to compare flow improvements at specific flow rates between the different models.

RESULTS AND DISCUSSION

CFD modelling calibration

The numerical model was calibrated by adjusting the roughness parameters until the predicted results aligned with the physical measurements. To evaluate the accuracy of the numerical models against the physical measurements, statistical indicators were calculated for each dataset. Residuals were defined as the difference between the physical and numerical headwater depth results for the same flow rate, as shown in Equation (8):

$$\text{Residual} = \text{Headwater depth}_{\text{Physical}} - \text{Headwater depth}_{\text{Numerical}} \tag{8}$$

From these residuals, the mean absolute error (MAE), root mean square error (RMSE), coefficient of variation (CV), and coefficient of determination (R^2) were derived to compare numerical results with physical measurements, as shown in Table 4.

The statistical assessment of the five wingwall and headwall angle configurations indicates consistently strong agreement between the numerical predictions and physical measurements. The mean residuals, expressed through the MAE, remain small across all cases. Negative mean values point to a slight tendency for overprediction of water levels in the numerical model, whereas positive values would reflect underprediction; however, these systematic errors are confined to a narrow range and are considered acceptable, since the MAE is a natural and unambiguous measure of average error (Willmott & Matsuura 2005). The RMSE values, varying between 7.7 and 11.7 mm, show that the average magnitude of deviations is small relative to the overall measurement scale (0–450 mm). Similarly, the CV values of 3.1–5.1% demonstrate that residual

Table 4 | Mean absolute error (MAE), root mean square error (RMSE), coefficient of variation (CV), and coefficient of determination (R^2) for physical and numerical modelling results

Wingwall and headwall model	Mean absolute error [MAE] (mm)	Root mean square error [RMSE] (mm)	Coefficient of variation [CV] (%)	Coefficient of determination (R^2)
90° wingwall; 90° headwall	−9.327	11.092	3.131	0.992
30° wingwall; 15° headwall	−8.098	11.721	4.114	0.993
30° wingwall; 30°headwall	0.282	7.695	3.748	0.996
45° wingwall; 45° headwall	−0.787	9.804	5.092	0.994
45° wingwall; 15° headwall	−6.324	10.334	4.304	0.994

variability is very low compared with the scale of the physical data. The coefficient of determination (R^2) values from a linear regression with the physical results plotted on the *y*-axis and the numerical predictions on the *x*-axis, all exceeding 0.992, confirm that the numerical models explain almost all of the variance observed in the physical results. Overall, these statistical indicators show that the models provide a very good fit, reproducing the physical behaviour with low scatter and relatively small errors.

The residuals expressed as a percentage of the physical measurements show that the majority of values lie within the range of −7 to +7%, as shown in Figure 5. This level of error is considered acceptable, as it reflects only small variations at both low and high headwater depths. At lower depths, fluctuations of approximately 5 mm were observed during the physical modelling study, corresponding to about 5%, while at higher depths, around 400 mm, fluctuations of roughly 30 mm were observed, representing less than 7% of the measured value. This demonstrates that, although the absolute residuals increase with water depth, the relative error remains consistently low across the entire range of measurements.

The close alignment between the numerical and physical modelling results made it possible to carry out further analysis of additional wingwall and headwall angles, as well as different rounded-edge inlets, using the numerical model.

Comparison with previous guidelines/studies

Headwater data obtained from the numerical analysis and the corresponding flow rates were used to generate performance curves. The experimental results are in good agreement with those reported in the literature (Herr & Bossy 1972; Boyd 1987; Charbeneau 2005; Marek 2009; Schall *et al.* 2012; SANRAL 2013; Austroads 2023). This comparison is shown for inlet control conditions in Figure 6.

Culvert wingwall and headwall analysis

Visualisation of the results in the scFLOW Post-Processor shows that the wingwall and headwall configurations influence culvert performance. For a 90° wingwall and 90° headwall at a flow rate of 54 l/s, a headwater depth of 376 mm was measured and the contraction after the inlet is clear in Figure 7(a). This corresponds to 841 l/s discharge and a 1.13 m headwater depth for the 600 × 600 mm prototype box culvert. A 30° wingwall and 30° headwall, shown in Figure 7(b)), showed no visible contraction after the culvert inlet and improved the headwater depth compared to the standard case for a similar flow rate, 57 l/s, measuring a headwater depth of 304 mm. This corresponds to 888 l/s discharge and a 0.91 m headwater depth for the prototype box culvert, representing a 0.22 m (20%) reduction in headwater depth.

Figure 8 shows all the results for the different headwall and wingwall configurations, with a third-degree polynomial trendline fitted to each inlet data set. A headwater depth of 1.2*D* is displayed as a threshold line since this is traditionally where flow changes from weir type to orifice type flow, and 2*D* is a criterion set by the South African National Roads Agency Limited (SANRAL 2013) for the maximum allowable headwater corresponding to a specific design recurrence interval.

The type of inlet improvement had a considerable influence once the inlet was submerged ($H_1 > 1D$), as shown in Figure 8. The 5° wingwall with a 5° headwall provided the greatest flow improvement overall for square box culverts, with a flow improvement of 20 l/s (35%) at a headwater depth of 2*D*. Applied to a 600 × 600 mm prototype box culvert, this configuration would discharge 1,215 l/s, resulting in a 312 l/s increase in capacity compared to the standard inlet. The second-best inlet was the 15° wingwall with a 15° headwall, which showed a flow improvement of 34%, followed by the 30° wingwall with a 15°

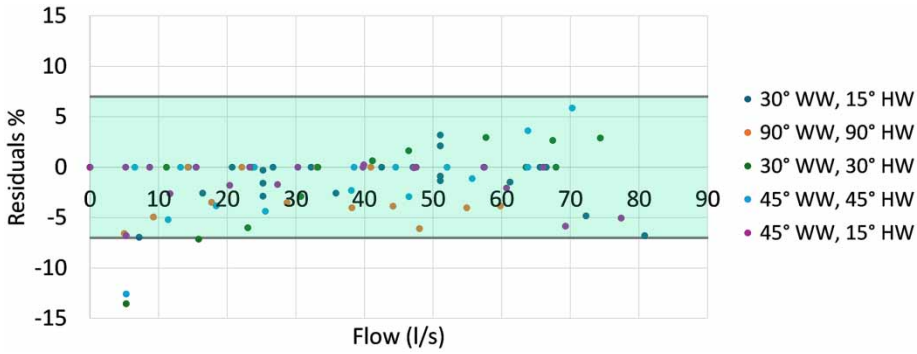

Figure 5 | Residuals of the physical and numerical results, lying within a bandwidth of −7 to +7%.

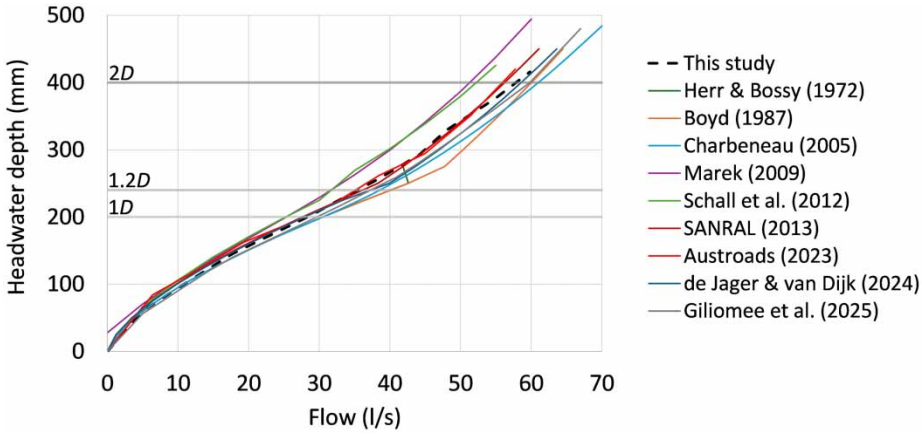

Figure 6 | Standard square-edge inlet box culvert equations from literature compared to the 90° wingwall and 90° headwall results.

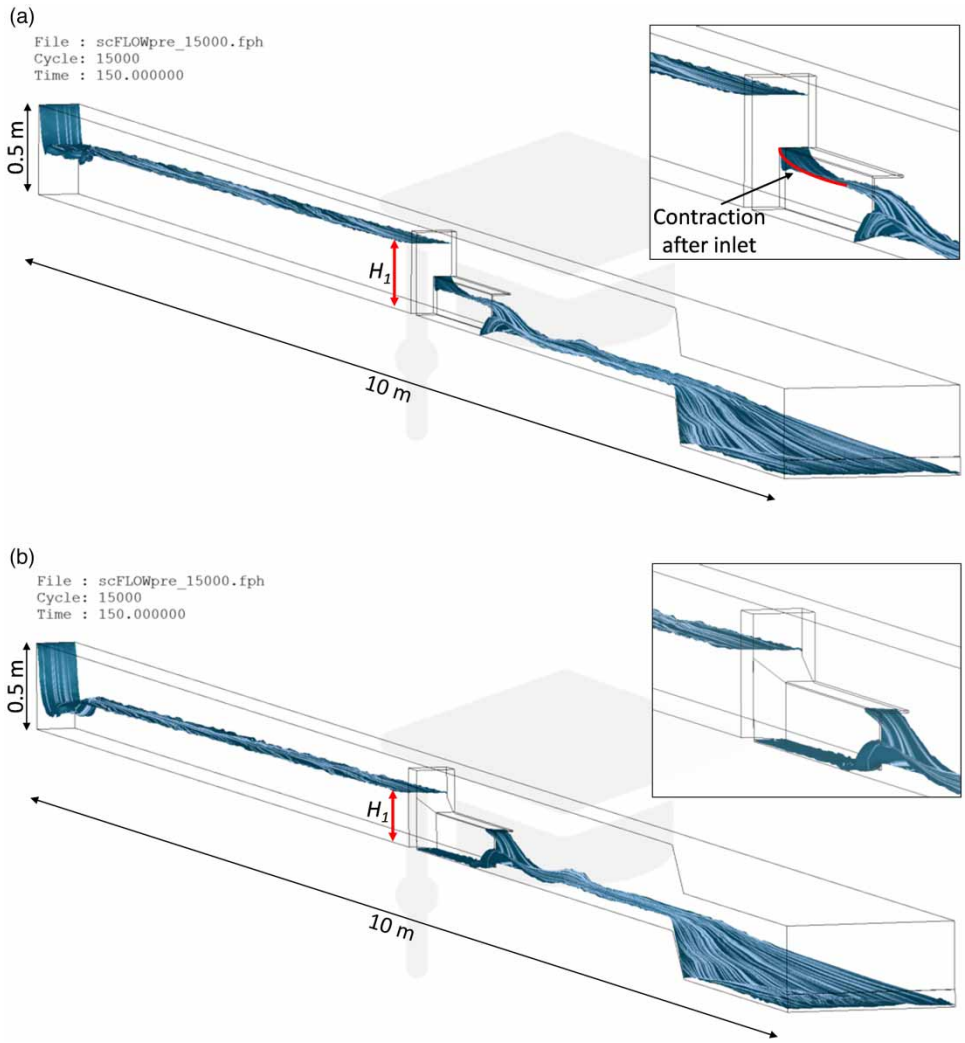

Figure 7 | (a) 90°wingwall and 90° headwall: 54 l/s measuring 376 mm headwater. (b) 30° wingwall and 30° headwall: 57 l/s measuring 304 mm headwater.

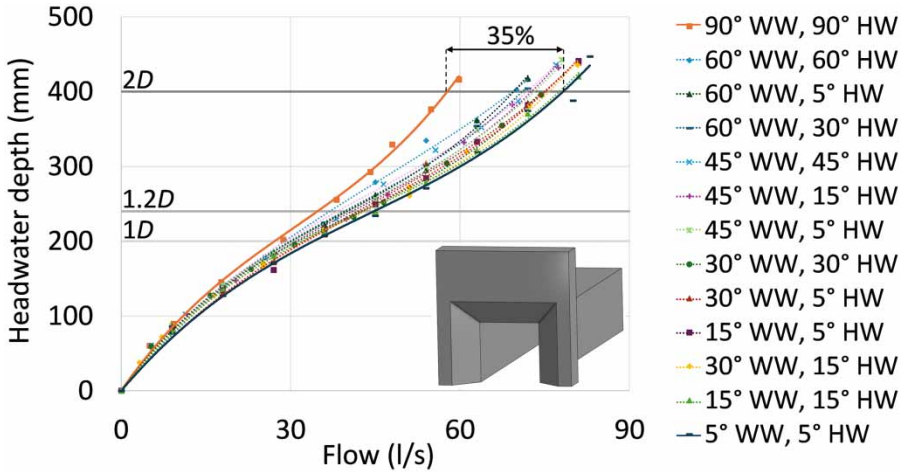

Figure 8 | Headwater to discharge relationship for different wingwall and headwall angles, ranked from least to most effective.

headwall, which showed a flow improvement of 31%, which was also identified as the best configuration by Giliomee *et al.* (2025) through physical modelling. This indicates that a decrease in wingwall and headwall angles increases flow capacity.

The percentage improvement for different wingwall and headwall angles applied to a square box culvert at a headwater depth of (a) 1.2*D* and (b) 2*D*, are shown in Figure 9. Smaller wingwall and headwall angles lead to greater improvement; however, the angles should be greater than 0°, which is the same as the 90° wingwall and headwall, standard square-edge inlet again. The optimal wingwall angle lies between 0 and 30°, and the optimal headwall angle lies between 0 and 15°.

The 5° wingwall with a 5° headwall extends 4.6*D* (920 mm) from the culvert barrel, making the 15° wingwall with a 15° headwall extending only 1.5*D* (300 mm) or the 30° wingwall with a 15° headwall extending only 0.7*D* (140 mm) a more practical solution, as shown in Figure 10. The optimal range, representing the least construction required for the greatest improvement, is shown by the orange-circled region in Figure 10. The construction cost should be considered with the improvement; however, the construction cost for an inlet modification is still much less than that of a complete rebuild and additional barrels.

Culvert rounded-edge inlet analysis

Figure 11 shows all the results for different rounded-edge inlet configurations, with a third-degree polynomial trendline fitted to each inlet data set.

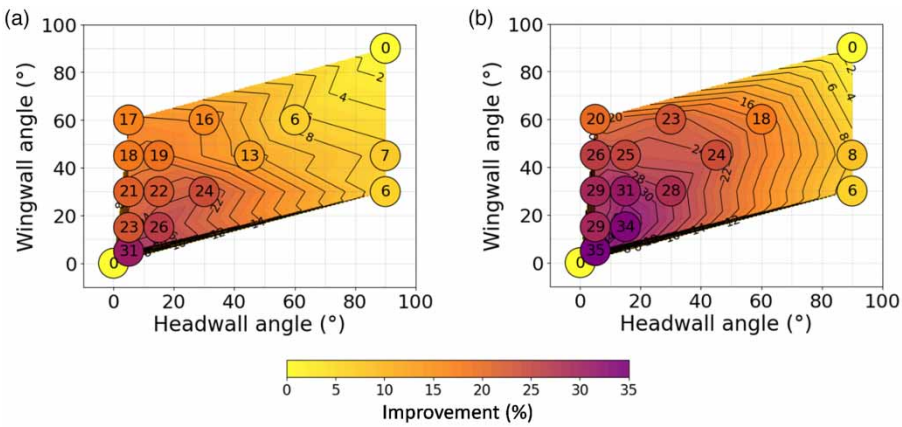

Figure 9 | Percentage improvement for different wingwall and headwall angles at a headwater depth of (a) 1.2*D* and (b) 2*D*.

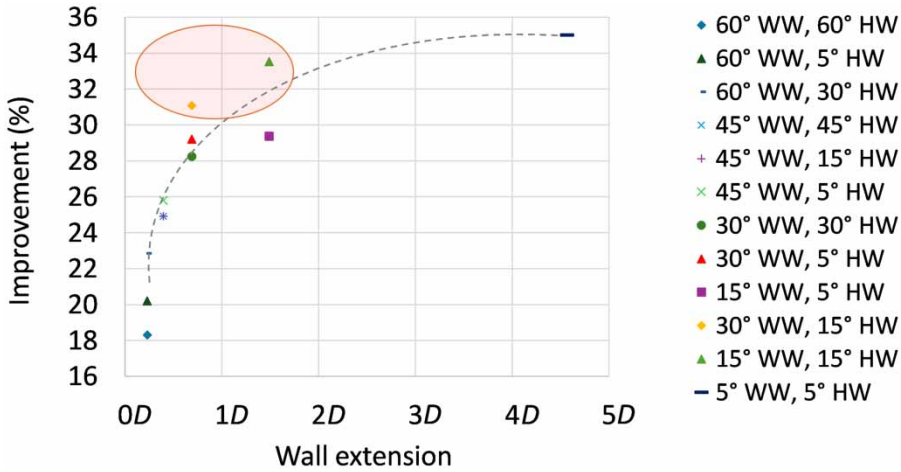

Figure 10 | Comparison between percentage improvement and the length of the wingwall and headwall construction upstream, in terms of *D*, culvert height.

The performance of a small, rounded-edge inlet (0.05*D*) does not differ significantly from that of a square-edged inlet, as shown in Figure 11. Rounded edges of ≥0.15*D* yield similar flow improvements, confirming the findings of Jaeger (2019) for circular culverts, who suggested that increasing the radius beyond 0.15*B* offers little additional improvement. The best rounded-edge inlets (0.15*D*-0.45*D*), which improved flow by up to 17 l/s (±30%), performed similarly to the fourth best wingwall and headwall angle configuration, a 15° wingwall with a 5° headwall. The best rounded-edge inlet retrofitted to a 600 × 600 mm prototype box culvert would discharge 1,169 l/s, representing a 265 l/s increase in capacity compared to the standard square-edge inlet.

CONCLUSIONS

The close alignment between the numerical and physical modelling results made it possible to investigate a wider range of inlet modifications, including more wingwall and headwall angles and different rounded-edge inlets. Furthermore, the numerical results for the standard square-edge inlet aligned closely with values reported in the literature, providing additional confidence in the modelling approach.

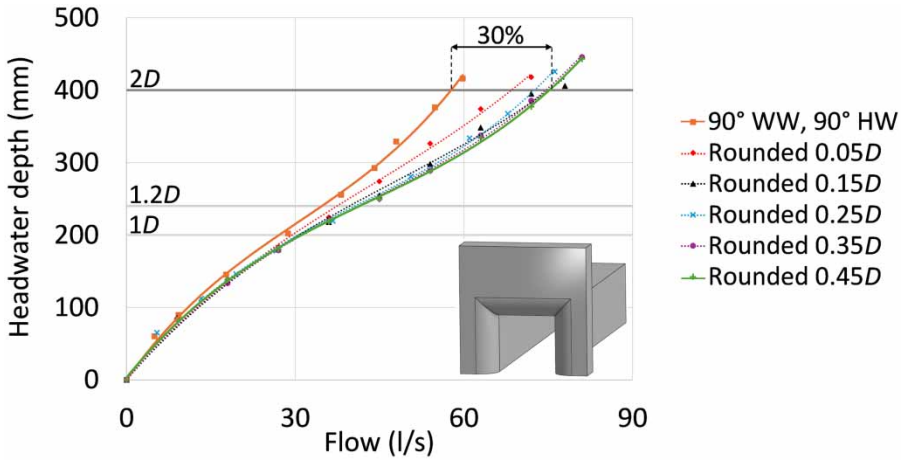

Figure 11 | Headwater to discharge relationship for different rounded-edge inlets applied to square box culverts, ranked from least to most effective.

From the numerical modelling results, the magnitude of improvement for the different culvert inlets was noticeable once the inlet was submerged. This is advantageous since the culvert conveys a large volume of water during high flood events, mitigating flooding. Optimised culvert inlets can increase flow capacity by up to 34% (for $H_1/D \geq 2$), which can eliminate the need to rebuild an entire inadequate culvert structure, offering a sustainable solution to increase culvert capacity. The smallest angles for both wingwalls and headwalls consistently provided the best performance. The 5° wingwall and 5° headwall provided the best performance but would be impractical to construct due to their large size. The second-best inlet, 15° wingwall and 15° headwall, offers similar flow improvements and is more feasible given its smaller size. Both these wingwall and headwall combinations achieved greater flow improvement than the best rounded-edge inlet (0.45D) applied to a square box culvert. Therefore, wingwalls and headwalls may be preferable to rounded edges, as they are already commonly used and often easier to construct; however, rounded edges may be easier and less expensive to retrofit onto existing culvert systems. These practical considerations highlight the value of assessing real-scale hydraulic performance. While the 15° wingwall and 15° headwall only improved the 200 × 200 mm model flow by 19.5 l/s, this translates to a 304 l/s increase at prototype scale (600 × 600 mm), demonstrating the performance benefit when applied in practice.

RECOMMENDATIONS

Further analysis is planned to determine the optimal balance between wingwall and headwall lengths, considering the overall size of culvert inlet construction. Therefore, cost benefits across different inlet types and scenarios should also be evaluated. It is recommended that tests should also be conducted under outlet control conditions.

The inlet improvements for box culverts in this study were based on a square culvert, which did not account for the exact contribution of a wingwall and a headwall for different sizes of rectangular culverts and should be considered in further research. It would also be useful to compare rectangular culverts with multi-barrel culverts of the same cross-sectional area, to evaluate how the flow improves through multiple openings when inlet modifications are applied. Since multi-barrels are commonly used, especially where the road level is very low, with limited fill height, it would be useful to evaluate the influence of wingwalls and headwalls with angles as determined in this study.

FUNDING

This work was supported by the South African National Roads Agency SOC Limited (SANRAL) (Project number: 1002-58600-2018-P7a.10).

DATA AVAILABILITY STATEMENT

All relevant data are included in the paper or its Supplementary Information.

CONFLICT OF INTEREST

The authors declare there is no conflict.

REFERENCES

Aly, T. E. (2017) Improving the pipe culvert efficiency by using inclined headwalls, *International Water Technology Journal, IWTJ*, **7** (1), 26–36.

Amback, B. C., Veróla, A. P., Sousa, M. M., Saraiva, L. E. S. & Miguez, M. G. (2025) A framework for urban planning structured by sustainable urban drainage: the proposal of a priority matrix for site selection, *Water Science & Technology*, **91** (10), 1185–1202. https://doi.org/10.2166/wst.2025.061.

Ashour, M. A., Aly, T. E. & Abdou, A. A. (2016) Inclined headwall is an efficient tool for maximizing the discharge efficiency through culverts, *3rd International Conference (Water Resources and Wetlands)*, Tulcea, Romania.

Austroads (2023) *Guide to Road Design Part 5B: Drainage – Open Channels, Culverts and Floodway Crossings*. Sydney, NSW: Austroads Ltd. AGRD05B-23.

Boyd, M. J. (1987) Generalised Head-Discharge Equations for Culverts, *Fourth National Local Government Engineering Conference*. Perth: The National Committee on Local Government Engineering of the Civil Colledge of the Institution of Engineers.

Bradley, J., Richards, D. & Bahner, C. (2005) *Debris Control Structures Evaluation and Countermeasures*. Salem, Oregon: U.S. Department of Transport FHWA.

Buck, G. & Allitt, R. (2019) The importance of culvert inlets, *Chartered Institution of Water and Environmental Management Urban Drainage Group Spring Conference 2019*, Dunblane Hydro, Scotland, 4.

Celik, I. B., Ghia, U., Roache, P. J. & Freitas, C. J. (2008) Procedure for estimation and reporting of uncertainty due to discretization in CFD applications, *Journal of Fluids Engineering-Transactions of the ASME*, **130** (7), 078001. https://doi.org/10.1115/1.2960953.

Charbeneau, R. J. (2005) *Hydraulics of Low-Headwater Box Culverts*. Austin, TX: Center for Transportation Research the University of Texas at Austin.

Cullis, J., Alton, T., Arndt, C., Cartwright, A., Chang, A., Gabriel, S., Gebretsadik, Y., Hartley, F., Jager, G. d., Makrelov, K., Robertson, G., Schlosser, C. A., Strzepek, K. & Thurlow, J. (2015) *An uncertainty approach to modelling climate change risk in South Africa World Institute for Development Economics Research*. WIDER Working Paper 45/2015. Available at: https://www.wider.unu.edu/publication/uncertainty-approach-modelling-climate-change-risk-south-africa.

de Jager, L. & van Dijk, M. (2024) Improvements to the hydraulic performance of culverts under inlet control conditions by optimisation of inlet characteristics, *Water*, **16** (11), 1569. https://doi.org/10.3390/w16111569.

Dutta, N., Kopparthi, P., Mukherjee, A. K., Nirmalkar, N. & Boczkaj, G. (2021) Novel strategies to enhance hydrodynamic cavitation in a circular venturi using RANS numerical simulations, *Water Research*, **204**, 117559. https://doi.org/10.1016/j.watres.2021.117559.

Feng, H., Du, S. & Zhu, D. Z. (2023) Numerical study of effects of flushing gate height and sediment bed properties on cleaning efficiency in a simplified self-cleaning device, *Water Science & Technology*, **88** (3), 542–555. https://doi.org/10.2166/wst.2023.245.

Giliomee, T. M. D., Loots, I. & van Dijk, M. (2025) Increasing culvert hydraulic capacity for improved climate resilience: a physical modelling analysis, *Water and Climate Change*, **16** (8), 2503–2518. https://doi.org/10.2166/wcc.2025.033.

Harrison, L. J., Morris, J. L., Normann, J. M. & Johnson, F. L. (1972) *Hydraulic Design of Improved Inlets for Culverts (Hydraulic Engineering Circular No. 13)*. Washington, DC: FHWA/EO-72-13. U.S. Department of Transportation, F. H. A.

Herr, L. A. & Bossy, H. G. (1972) *Capacity Charts for the Hydraulic Design of Highway Culverts*. Washington, DC: Federal Highway Administration. 20590. TRANSPORTATION, U. S. D. O.

Hexagon (2024) *scFLOW User's Guide: Analysis Method*. Osaka, Japan: Software Cradle Co., Ltd.

Hirt, C. W. & Nichols, B. D. (1981) Volume of fluid (VOF) method for the dynamics of free boundaries, *Journal of Computational Physics*, **39** (1), 201–225. https://doi.org/10.1016/0021-9991(81)90145-5.

Iaccarino, G., Ooi, A., Durbin, P. A. & Behnia, M. (2003) Reynolds averaged simulation of unsteady separated flow, *International Journal of Heat and Fluid Flow*, **24** (2), 147–156. https://doi.org/10.1016/S0142-727X(02)00210-2.

Iwamoto, S., Fujimoto, R., Sakaue, K. & Mitsunaga, T. (2023) Study on simulation of building drainage systems by CFD Part 1 Verification based on existing experimental results, *2023 Symposium CIB W062*. Leuven, Belgium.

Jaeger, R. (2019) *Hydraulic Improvements in Culverts for Climate Change Adaptation*. *Doctor of Philosophy Doctor of Philosophy*, University of the Sunshine Coast, Sunshine Coast, Australia.

Jones, J. S., Kerenyi, K. & Stein, S. (2006) *Effects of Inlet Geometry on Hydraulic Performance of Box Culverts*. Springfield, VA: U.S. Department of Transportation, Federal Highway Administration.

Marek, M. (2009) *Hydraulic Design Manual.Texas. Design Division (DES)*. Austin, TX: Texas Department of Transportation.

Martin, M. B., Pinon, G., Barajas, G., Lara, J. L. & Reveillon, J. (2023) Computations of pressure loads on an oscillating water column with experimental comparison for random waves, *Coastal Engineering*, **179**, 104228. https://doi.org/10.1016/j.coastaleng.2022.104228.

Marum, V. J. d. O., Reis, L. B., Maffei, F. S., Ranjbarzadeh, S., Korkischko, I., Gioria, R. d. S. & Meneghini, J. R. (2021) Performance analysis of a water ejector using Computational Fluid Dynamics (CFD) simulations and mathematical modeling, *Energy*, **220**, 119779. https://doi.org/10.1016/j.energy.2021.119779.

Menter, F. R. (1994) Two-equation eddy-viscosity turbulence models for engineering applications, *AIAA Journal*, **32** (8), 1598–1605. https://doi.org/10.2514/3.12149.

Morrow, J. D. P. (2020) *The Basics of Culvert and Inlet Design*. Fairfax, VA: PDH Center.

Quang, C. N. X., Giang, N. N. H., Hoa, H. V. & Hung, P. Q. (2022) Effects of sediment deposit on the hydraulic performance of the urban stormwater drainage system, *IOP Conference Series: Earth and Environmental Science*, **964**, 012020. IOP Publishing. https:/doi.org/10.1088/1755-1315/964/1/012020.

ROCLA (2017) *Rocla Product Catalogue*. Rocla (Pty) Ltd., South Africa. https://www.rocla.co.za/wp-content/uploads/2018/08/rocla-product-catalogue.pdf.

SANRAL (2013) *The South African National Roads Agency SOC Limited Drainage Manual*. Pretoria: The South African National Roads Agency SOC Limited.

Schall, J. D., Thompson, P. L., Zerges, S. M., Kilgore, R. T. & Morris, J. L. (2012) *Hydraulic Design of Highway Culverts Third Edition, Hydraulic Design Series Number 5*. Colorado: FHWA-HIF-12-026. TRANSPORTATION, U. S. D. O.

Simscale (2025) *K-Omega Turbulence Models* [Online]. Available at: https://www.simscale.com/docs/simulation-setup/global-settings/k-omega-sst/ [Accessed 23 August 2025].

Straub, L. G., Anderson, A. G. & Bowers, C. E. (1953) *Importance of Inlet Design on Culvert Capacity*. Minneapolis, Minnesota: University of Minnesota.

Ueyama, A. (2019) *Want to Know More! Basics of Thermo-Fluid Analysis 18: Chapter 3 Flow 3.4.1 Steady-State Flow and Transient Flow [Online]*. Osaka, Japan: Hexagon Cradle Software. Available at: https://www.cradle-cfd.com/media/column/a151 [Accessed 23 August 2025].

van der Werf, J. A., Pons, V., Smythd, K., Shi, B., Lechevallierg, P., Abdallai, E. M. H., Andrusenkoa, E., Broekhuizen, I., Cavadini, G. B., Morenoa, A. F. C., Cristianoj, E., D'Ambrosiok, R., Drostea, A. M., Evangelistil, M., Fernandesm, G., Garzóna, A., Giroto, E., Guericke, L., Liaoq, W., Mazzoglior, P., Mittala, A., Müller, A., Naves, J., Oberaschert, M., Okwori, E., Perez-Alvarinov, J. I., Pritsis, S., Regueiro-Picallos, M., Roghani, B., Taguchix, V. J., Waniy, O., Wei, H., Yıldızlı, T. & Yerima, H. Z. (2025) Flooded with potential: urban drainage science as seen by early-career researchers, *Water Science & Technology*, **91** (7), 861–875. https://doi.org/10.2166/wst.2025.045.

Versteeg, H. K. & Malalasekera, W. (2007) *An Introduction to Computational Fluid Dynamics the Finite Volume Method, 2/E*. Harlow, England: Pearson Education Limited.

West, E. M. (1956) *Hydraulic Model Studies of Culvert Operation*. Lexington, Kentucky: Kentucky Transportation Center.

Willmott, C. J. & Matsuura, K. (2005) Advantages of the mean absolute error (MAE) over the root mean square error (RMSE) in assessing average model performance, *Climate Research*, **30**, 79–82. https://doi.org/10.3354/cr030079.

Yarnell, D. L., Nagler, F. A. & Woodward, S. M. (1926) *Flow of Water Through Culverts. Iowa*. Iowa City, IA: University of Iowa Studies in Engineering.

First received 2 September 2025; accepted in revised form 21 January 2026. Available online 6 February 2026